Title
Nitrogen mustard-induced corneal injury involves the sphingomyelin-ceramide pathway

Journal
The Ocular Surface, 16(1)

ISSN
1542-0124

Authors
Charkoftaki, Georgia
Jester, James V
Thompson, David C
et al.

Publication Date
2018

DOI
10.1016/j.jtos.2017.11.004

Peer reviewed

HHS Public Access

Author manuscript

Ocul Surf. Author manuscript; available in PMC 2020 July 23.

Published in final edited form as:

Ocul Surf. 2018 January ; 16(1): 154–162. doi:10.1016/j.jtos.2017.11.004.

Nitrogen mustard-induced corneal injury involves the sphingomyelin-ceramide pathway

Georgia Charkoftaki[a], **James V. Jester**[b], **David C. Thompson**[c], **Vasilis Vasiliou**[a,d,*]

[a]Department of Environmental Health Sciences, Yale School of Public Health, New Haven, CT, USA

[b]Gavin Herbert Eye Institute, University of California, Irvine CA, USA

[c]Department of Clinical Pharmacy, Skaggs School of Pharmacy & Pharmaceutical Sciences, University of Colorado, Aurora, CO, USA

[d]Department of Ophthalmology and Visual Science, Yale School of Public Health, New Haven, CT, USA

Abstract

Purpose: Nitrogen mustard (NM), which simulates the effects of sulfur mustard (SM), is a potent vesicant known to cause irreversible corneal damage. This study investigates the mechanisms by which NM induces corneal damage by examining the impact of NM exposure on the morphology and lipidome of the cornea.

Methods: Intact *ex vivo* rabbit eyes were placed in serum-free DMEM organ culture. NM (0, 1, 2.5, 5 or 10 mg/ml) was applied to the central cornea for 5,10 or 15 min using a 5 mm filter disk and subsequently rinsed with DMEM. Corneas were then cultured for 3, 24, or 48 h before being fixed for morphological analysis or for 24 h before being snap frozen for lipidomic analysis.

Results: No morphological changes were detected 3 h after NM exposure. Twenty-four h after exposure, 1 mg/ml NM caused erosion of the corneal epithelium, but no damage to the underlying stroma. Damage caused by 2.5 mg/ml NM extended almost two thirds through the corneal stroma, while 5 mg/ml completely penetrated the corneal stroma. An altered lipid profile occurred 24 h after corneas were exposed to NM. Specific sphingomyelins, ceramides, and diacylglycerols were increased up to 9-, 60- and 10-fold, respectively.

Conclusions: NM induces concentration- and exposure time-dependent damage to the cornea that increases in severity over time. Alterations in the sphingomyelin-ceramide pathway may contribute to the damaging effects of NM exposure.

*Corresponding author. Department of Environmental Health Sciences, Yale School of Public Health/Yale School of Medicine, 60 College Street, Rm. 511, New Haven, CT 06520-8034, USA. vasilis.vasiliou@yale.edu (V. Vasiliou).

Appendix A. Supplementary data

Supplementary data related to this article can be found at https://doi.org/10.1016/jjtos.2017.11.004.

Conflict of interest

The authors have no commercial or proprietary interests in any concept or product discussed in this article.

Keywords

Cornea; Depth of injury; Metabolomics; Nitrogen mustard; Sulfur mustard

1. Introduction

Sulfur mustard (SM, bis[2-chloroethyl]sulfide) is a potent, highly reactive, lipophilic vesicant [1–3]. It is highly volatile at room temperature and, due to its lipophilicity, is a very persistent contaminant of the environment, especially of the soil [4].

Sulfur mustard is a chemical warfare agent, which was first used during World War I (WWI). It has been the most widely used chemical weapon and was used heavily during the Iran-Iraq war [5]. Existing large stockpiles of SM pose a continuous risk to military and civilian populations residing near their sites of storage, in addition to their potential use in warfare and terrorism [4].

Sulfur mustard can cause injury to organs (including the skin, eyes, and respiratory tract) that can take several months to heal [6,7]. When used as a volatile chemical weapon, the eye is the most susceptible to SM-related injuries compared to the target organs, the skin, and respiratory tract [8]. Due to its highly alkylating properties, SM exerts a local toxic effect on the eyes by rapidly reacting with major cellular molecules [9]. The severity of the ocular injury depends on the concentration and the time of exposure [10]. Symptoms may occur up to 12 h post-exposure. Usually, an acute phase occurs initially, manifesting clinically as photophobia, inflammation of the anterior segment, and corneal erosions. This may be followed by irreversible corneal injuries that progress to vision impairment and, potentially, blindness [11].

Studies investigating ocular SM exposure have reported histopathological changes of the cornea, including ulceration, keratocyte death, inflammation, stromal neovascularization, and blistering [12–14]. The mechanisms by which these deleterious effects occur have been proposed to include induction of oxidative stress and lipid peroxidation, and cell damage associated with SM alkylation of DNA. This has also been linked to glutathione (GSH) depletion possibly leading to oxidative stress and lipid peroxidation [15–18].

However, the concentration or the time of the exposure needed to trigger the pathophysiological effects after SM exposure have not been fully elucidated yet, leading to unsuccessful treatments. The present study uses nitrogen mustard (NM), which has structural and toxicological properties that are similar to SM and can been used as a surrogate [19–21]. The aim of the present study was to (i) characterize corneal damage induced by (NM), in the *ex vivo* isolated rabbit eye, and (ii) assess the impact of NM exposure on the metabolic profile of the cornea using untargeted lipidomics.

2. Methods and materials

2.1. Methods

2.1.1. Isolated rabbit eye testing—The methods used for these studies were based on a previous published model for the detection of ocular irritation in isolated rabbit eyes [22]. Eyes with intact eyelids from rabbits aged 8–12 weeks were received from a "slaughter house" from Pel Freez Biologicals (Rogers, AR), and shipped overnight on ice in serum-free Dulbecco's Modified Eagle's Medium (DMEM). Upon receipt, eyelids were surgically removed, and the eyes were subsequently washed in sterile, serum-free and phenol red-free DMEM with low glucose (pH 7.2) (Sigma-Aldrich, St. Louis, MO) supplemented with antibiotic/antimycotic agents (Life Technologies, Grand Island, NY). Eyes were then placed in a 12-well tissue culture plate (Costar, Corning Inc, Corning, NY), cornea side up. Approximately 1 ml phenol red-free DMEM was added to each well without submerging the cornea. To restore corneal transparency and normal thickness, eyes were then incubated for 2 h in a humidified, 5% CO_2 tissue culture incubator maintained at 37 °C. Eyes were then examined using a dissecting microscope (Zeiss Discovery V12 Stereo Microscope (Gottingen, Germany)) for signs of damage; any corneas showing ocular lesions were removed from the study.

Under a chemical hood, liquid NM (mechlorethamine hydrochloride, Sigma-Aldrich, St. Louis, MO) was dissolved in sterile water to create various concentrations (0.01–100 mg/ml). Ten μl NM solution or vehicle (sterile water) was applied to a sterile 5 mm diameter #1 filter disc (Whatman International Ltd, Maidstone, England), which was then placed onto the central cornea for various exposure times (10 s - 1 h [Fig. 1A]). Eyes were then rinsed with 20 ml sterile DMEM, placed back into the 12-well tissue culture plate and in the incubator for 3 h. At the end of this period, the cornea (including 2–3 mm of the adjoining sclera) from each eye was surgically removed. Some corneas were then draped over an agar post, (comprised of 2% low melting temperature agarose (SeaPaque Agarose, Lonza, Rockland, ME) in DMEM) (Fig. 1B), fresh sterile media was added to the well without submerging the cornea, and cultured for 24 or 48 h post-exposure period. Corneas were collected at 3 h (i.e., immediately after surgical removal of the cornea), 24 h or 48 h post exposure and fixed overnight in 2% paraformaldehyde (Electron Microscopy Sciences, Hatfield, PA) in phosphate buffered saline (pH 7.4) (PBS). Each vehicle and NM concentration, exposure duration and post-exposure duration was conducted in at least 3 corneas.

2.1.2. Tissue processing and fluorescent labeling—After overnight fixing, a 3 mm wide, central strip of cornea was isolated by trimming and placed in cold (4 °C) sucrose (15% w/v) solution for 4 h. The corneal strip was then transferred to 30% (w/v) sucrose and stored overnight at 4 °C. The corneal tissue was subsequently embedded in O.C.T. Compound (Tissue-Teck, Sakura Finetek, Torrance, CA), snap-frozen in liquid nitrogen and stored at −80 °C (Revco Ultima II ultrafreezer, Asheville, NC). The tissue was then sectioned (Leica CM 1850 crytome, Leica, Wetzlar, Germany) to produce six 8-μm-thick tissue sections collected at 100 μm intervals. Three sections were mounted onto a glass slide, and stained for 1 h with Alexa 488 Phalloidin (Invitrogen, Eugene, OR) using 10 units per

section diluted in PBS. Sections were then counterstained with 4 ′,6-diamidino-2-phenylindole (DAPI) (300 nM, Sigma-Aldrich) in PBS for 15 min and a coverslip was subsequently placed over the tissue sections using Gel/Mount (Biomeda, Foster City, CA) mounting media.

2.1.3. Tissue and damage analysis—Stained tissue sections were subjected to fluorescence microscopy (Leica DM16000B, Leica-Microsystems). Images of DAPI (Ex/Em = 358/461) and phalloidin (Ex/Em = 488/530) fluorescence were captured using a 12-bit monochromatic QlClick CCD camera (Qlmaging, Surrey, BC, Canada) and Metamorph digital imaging software (Molecular Devices, Sunnyvale, CA). For each section, tiled images were taken over the central 1–2 mm of the cornea; the images were stitched together using Metamorph (Molecular Devices, Sunnyvale, CA). Images of both DAPI (nuclei) and phalloidin (live cells) fluorescence were obtained for each section. Using phalloidin staining as a marker of live cells, the epithelial thickness and region of dead, non-phalloidin stained, stroma (S_{DEAD}) were measured. Total stromal thickness (S_{TOTAL}) was measured in each section using the DAPl-stained nuclear fluorescence. At least three regions separated by 250–500 mm were measured to estimate the epithelial thickness, stromal thickness and depth of injury (Dol) using the following formula:

$$\text{Stromal DoI} = \frac{S_{DEAD}}{S_{TOTAL}} \text{ (expressed as a percentage)}$$

2.1.4. Statistics—Statistical analyses were conducted using SigmaStat for Windows 3.11 (Systat Software Inc., Point Richmond, CA). For each eye, the average epithelial and stromal thicknesses, and Dol were calculated from the three sections. The effect of treatment (vehicle or NM) was calculated using at least 3 eyes. Comparisons between treatments were made using a one-way Analysis of Variance, with $P < 0.05$ being considered significant. Data are presented as mean ± SD.

2.1.5. Untargeted lipidomics

2.1.5.1. Sample preparation.: Corneal buttons were exposed to vehicle (sterile water) (n = 6), 5 mg/ml (n = 6) or 10 mg/ml NM (n = 6) for 15 min and harvested at 24 h. The tissues were then snap frozen and processed for lipidomics. Corneal tissue was pulverized (MultiSample BioPulverizer Cryogenic Tissue Crusher) and 35–45 mg of tissue was collected, quenched in (chloroform: methanol 1:1) following a modified Folch's method [23] with the extraction solvent being normalized to tissue weight (25 μl/mg tissue). Then, the tissue samples were shaken in an orbital shaker for 1 h in room temperature and the lipid fraction obtained from the dual phase extraction [23] was concentrated in a SpeedVac concentrator (Savant, SPD 111V, Thermo Scientific). The dried-down samples were reconstituted in isopropanol:acetonitrile:- water (2:2:1), containing 5 μl of SPLASH™ Lipidomix® Mass Spec Standard (Avanti Polar Lipids, lnc.) and analyzed using a UPLC-MSE approach (ramped collision energy, 15–40V).

2.1.5.2. Liquid chromatography.: All samples were randomized, run in triplicate and injected onto an Acquity BEH C18 (1.7 μm, 2.1 mm × 100 mm) column (Waters). A pooled

sample containing 10 μl of each individual sample was injected every five injections for quality control (QC). The mobile phase involved a gradient comprising varying amounts of solutions A (10 mM ammonium formate in 60% v/v acetonitrile) and B (10 mM ammonium formate in 95% isopropanol and 5% acetonitrile). The linear gradient elution was: 40–43% B (020132 min), 43–50% B (over 0.1 min), 50–54% B (over 10 min), 54–70% B (over 0.1 min), 70–99% B (over 5.9 min), 99–40% B (over 0.1 min), and 40% B (for 2 min), run at 300 μl/min in positive Electrospray Ionization mode and the column temperature was maintained at 55 °C. Samples were analyzed using a Waters XEVO-G2-XS QTOF mass spectrometer. In all cases, the mass spectrometer was set to acquire over the range 50–1200 m/z.

2.1.6. Data analysis—Mass spectrometer data were uploaded and processed on Progenesis Ql Software (Nonlinear Dynamics, Waters) for peak peaking and mass spectral alignment. Statistical analysis was performed on the metabolite features using EZinfo software (Nonlinear Dynamics, Waters). $P < 0.05$ was considered significant. The q-value was used to eliminate false positives. Multivariate analyses were performed using the Simca program (Umetrics, Umea, Sweden). Statistically significant metabolites (FDR, $q < 0.05$) were identified using putative identifications as compared to those metabolites housed on the LipidBlast database [24].

2.2. Materials

All the solvents used for metabolomics were of LC-MS grade: acetonitrile Baker Analyzed™ Ultra LC/MS (J.T. Baker™), methanol Baker Analyzed® LC/MS Reagent (J.T. Baker™), formic acid 99.5+%, Optima™ LC/MS Grade, (Fisher Chemical) and chloroform (Fisher Chemical).

3. Results

3.1. Morphology

In corneas exposed to sterile water, there was no change in phalloidin staining of the corneal epithelium or stroma at 3, 24 or 48 h post-exposure (Fig. 1C–E). All such vehicle-exposed corneas showed strong phalloidin staining of the corneal epithelium, weaker staining of the stromal keratocytes, and stronger staining of the posterior corneal endothelium. The corneal epithelium maintained a normal stratified appearance, with 5–7 cell layers comprised of basal epithelial cells with overlying wing and superficial cells.

In preliminary studies, brief exposure (10s) of isolated rabbit eyes to various concentrations of NM (0.01–100 mg/ml) followed by immediate washing of the corneal surface showed no change in phalloidin staining, suggesting no damage at 3, 24, or 48 h after exposure (data not shown). Corneas exposed to 1 or 10 mg/ml NM for 5 min showed normal phalloidin staining of the corneal epithelium and stroma 3 h after exposure (Fig. 2A, D). Twenty-four and 48 h after exposure, corneas exposed to 1 mg/ml NM continued to show no loss of corneal epithelial phalloidin staining (Fig. 2B and C), while those exposed to 10 mg/ml NM showed severe damage to the corneal epithelium and swelling of the corneal stroma, leading to the extensive thickening of the cornea (Fig. 2E and F).

To produce a range of NM-induced corneal damage, corneas were exposed to different concentrations of NM (1.0, 2.5, and 5.0 mg/ml) at different exposure times (5, 10 and 15 min). Eyes were then placed in organ culture and fixed 24 h post-exposure. The effects of concentration and exposure time on epithelial thickness, stromal thickness, and DoI were then measured, and the results are shown in Fig. 3. In general, increasing concentration and increasing exposure time to NM led to progressively increased damage to the central cornea (Supplementary data). For the shorter exposure duration examined (5 min), 5 mg/ml was the only NM concentration that caused discernible changes in the cornea, specifically as thickening of the stroma (Fig. 3B). Increasing the exposure time resulted in the appearance of corneal damage manifested as thinning of the epithelium, thickening of the stroma, and an increase in stromal depth of injury (Fig. 3A–C). At the lower NM dose (1 mg/ml), no significant changes were detected in corneas exposed for 5,10, or 15 min, although slight damage to the cornea (as reflected in loss of superficial epithelial cells) and a distortion of the normal stratified epithelial layer was observed in corneas exposed for 10 min (Fig. 4A, inset). Exposure to 2.5 mg/ml NM for 10 min resulted in more extensive damage to the cornea, manifesting as erosion of the epithelium (Fig. 4B inset) and significant epithelial thinning. The stroma also showed cell damage (Fig. 4B, double arrowhead), leading to an average 64% DoI with significant stromal thickening. Corneas exposed to 5 mg/ml NM showed the greatest damage, with complete erosion of the epithelium (Fig. 4C, inset) and significant epithelial thinning (Fig. 3A). Stromal injury was also greater, extending to 100% in many regions (Fig. 4C, double arrowhead) and averaging 93% DoI (Fig. 3C), with significant stromal thickening that was perhaps related to damage to the corneal endothelium. Exposing corneas to NM for 15 min resulted in no further increases in DoI (Fig. 3).

3.2. Untargeted lipidomics

Untargeted lipidomics was performed to determine the variation in metabolic profiles between the different NM exposures of the cornea. Comprehensive profiles were acquired from tissue extracts. A total of 5455 features were detected, of which 210 were significantly altered in the NM-exposed samples (FDR, $q < 0.05$). In order to visualize and identify the most prominent metabolic differences between the various NM exposures, orthogonal partial least square discriminant analysis (OPLS-DA) was performed. Fig. 5 displays the separation between the various NM exposure groups along the first principal component, indicating relevant differences in their basal metabolic activities.

The lipids altered by NM exposure included sphingomyelins, ceramides, diacylglycerols, and platelet activating factor. The putatively-identified sphingomyelins (listed in Table 1) were increased between 2.1- and 9.3-fold in the extract from NM-exposed cornea (Fig. 6A). The largest increase (9.4-fold) was observed for $C_{46}H_{93}N_2O_6P$ (m/z: 801.6855) ($q = 1.43 \times 10^{-4}$) in corneas exposed to 10 mg/ml NM. All of the increases in sphingomyelins were almost three times higher in samples from 10 mg/ml NM-exposed corneas than in 5 mg/ml NM-exposed corneas. The two exceptions were $C_{47}H_{95}N_2O_6P$ (m/z: 815.7009) and $C_{49}H_{97}N_2O_6P$ (m/z: 841.7169) in which the fold changes were very similar for both concentrations of NM (Fig. 6A). In addition, several putatively-identified ceramides were increased in extracts from corneas exposed to 5 or 10 mg/ml NM. Both C18 (d:18:1/18:0)

and C20 (d:18:1/20:0) ceramides were generally increased to a similar extent by both NM concentrations (1.7–4.0 fold), with the exception of C20 (d18:1/20:0) which was not increased by 5 mg/ml NM (Fig. 6B). C22 (d:18:1/22:0) ceramide increased to the greatest extent of all metabolites with a 22-fold and 59-fold change in the corneas exposed to 5 and 10 mg/ml NM exposure, respectively (Fig. 6B). Diacylglycerols (DAGs) were also increased between 1.7- and 10-fold by NM exposure (Fig. 6C). The increase in all DAGs was greater in corneas exposed to 10 mg/ml NM than 5 mg/ml NM (Fig. 6C). Platelet activating factor (PAF) was also increased 3.2- and 3.5-fold in corneas exposed to 5 or 10 mg/ml NM, respectively (Fig. 6D).

4. Discussion

Exposure to sulfur mustard damages cells and tissue due to its ability to alkylate cellular molecules. Although it was developed almost a century ago, the mechanisms responsible for corneal mustard injury are not clearly understood. In the experiments described herein, isolated rabbit corneas were placed in organ culture and exposed to the NM for various durations. The pathophysiological and biochemical sequelae of NM exposure were detected utilizing histological analyses (e.g., DoI) and untargeted lipidomics.

In the present study, phalloidin staining was used to measure the corneal DoI. An advantage of this procedure is that it is relatively fast (i.e., less than 1 h incubation time) and more cost-effective than TUNEL labeling and has been shown to measure the same depth of injury [22]. Twenty-four h after exposure to NM, the cornea underwent extensive thickening that was characterized by thinning of the epithelium and thickening of the stroma. The changes to the cornea were both concentration- and exposure duration-dependent such that the effects manifested at higher concentrations (2.5 or 5 mg/ml) and for durations greater than or equal to 10 min. While 1 mg/ml NM did not alter corneal epithelium thickness, immunohistochemistry revealed loss of superficial epithelial cells. Higher NM concentrations caused more extensive erosion of the epithelium and loss of stromal cell viability. These deleterious stromal cell changes also occurred in a concentration-dependent manner and are reflected in the increasing DoI that attended higher NM concentrations. These results clearly show that the concentration and the duration of exposure contribute to the severity of the corneal damage induced by NM. It is noteworthy that the post-exposure time also influenced the severity of corneal damage. For example, no damage to the corneal epithelium or stroma was observed 3 h after exposure to 10 mg/ml NM for 5 min. However, severe damage to the stroma and extensive thickening of the cornea was observed at latter post-exposure time points, i.e., 24 or 48 h. As such, it is apparent that the injurious effects of NM exposure take time to develop. It should also be noted that extensive stromal swelling was likely due to damage to the corneal endothelium, allowing for loss of corneal deturgesence. Sulfur mustard vapor-induced endothelial injury has been previously noted by McNutt [25] Although endothelial damage was not specifically measured in the present study, endothelial cell loss was detected in corneas showing deep stromal injury. Given that the corneas were draped over agar posts in our study, it is possible that handling of the corneas during processing may have contributed to the observed endothelial damage. Further studies are needed to more specifically evaluate the acute effects of NM exposure on endothelial function.

In order to explore the biochemical consequences of NM exposure, the effects of NM concentrations that caused corneal damage (5 and 10 mg/ml) on corneal cell metabolite formation were examined using untargeted lipidomics. This approach revealed members of the sphingomyelin-ceramide metabolic pathway to be increased by NM. These included select sphingomyelins, ceramides, diacylglycerols, and platelet activating factor.

Information on the role of these lipids in corneal cell physiology and pathology is quite limited. A recent study linked the increased levels of apoptosis-related proteins to corneal thinning in keratoconus (KC) [26], showing that certain proteins, as well as abnormal lipid metabolism, and cell death are major keratoconic processes. Keratoconus is a corneal disorder that involves thinning of the corneal stroma and protrusion of the cornea leading to progressive astigmatism and impaired vision [27]. Later stages of the disease can also involve corneal scarring that can lead ultimately to loss of vision [28]. All of these KC symptoms bare some similarity to the ones occurring in the cornea after NM exposure, especially epithelial thinning and corneal haze [28]. Moreover, apoptosis seems to play a major role in epithelial-induced injury.

For example, keratocyte apoptosis occurs in the corneal stroma as a result of injury or exposure to ultraviolet radiation [29–31]. Keratocytes are the precursor cells for myofibroblasts, which are responsible for successful wound repair and regeneration of normal corneal structure and function. Failure of successful corneal healing by myofibroblasts leads to corneal stromal opacity (fibrosis) and vision impairment [32,33]. As such, apoptosis may significantly contribute to the observed corneal damage induced by NM exposure, and explain corneal epithelial thinning, keratocyte cell death and stromal thickening [32]. In the present study, corneas exposed to NM generated increased levels of sphingomyelins, ceramides, diacylglycerols, and platelet activating factor. Ceramides induce apoptosis in primary cultures of rabbit corneal fibroblasts [34] and cell death in human corneal stromal fibroblasts [35]. Platelet activating factor inhibits corneal wound healing by inducing stromal keratocyte apoptosis and upregulating matrix metalloproteinases [36]. Recently published work involving human corneal fibroblasts from normal and KC patients revealed increased concentrations of sphingolipids and ceramides [28]. Elevated ceramide levels have been associated with apoptotic pathways, and appear to induce death signals and inhibit the cell survival pathway. In the present study, select ceramide levels were increased by NM, especially C22 (d:18:1/22:0) which was increased almost 60-fold by 10 mg/ml NM. Several diacylglycerols were also increased by NM exposure. These are generated during the formation sphingomyelin from ceramide by sphingomyelin synthases. The nascent state of knowledge regarding the biological actions of specific metabolites of the sphingomyelin-ceramide pathway, it is not possible to identify whether the changes in a specific lipid observed in the present study contribute to the corneal injury induced by NM exposure.

5. Conclusions

Our results have shown that the corneal damage caused by NM depends on its concentration, and the duration of the exposure. Various levels of corneal injury were observed, from thinning to complete erosion of the corneal epithelium. Using an untargeted lipidomics approach, we were able to show that NM exposure causes significant changes in the lipid

profile of the cornea and such changes may contribute to the adverse effects of NM exposure. The sphingomyelin-ceramide pathway has not been previously implicated in corneal damage induced by NM. Further investigations are needed to determine the contribution of specific sphingomyelin-ceramide-derived lipids to NM-induced corneal injury.

Supplementary Material

Refer to Web version on PubMed Central for supplementary material.

Acknowledgement

This work was supported by the National Institutes of Health (NIH) Grant EY026776 (VV), AA022057 (VV) and an unrestricted grant from Research to Prevent Blindness, Inc. (JVJ).

References

[1]. Panahi Y, Rajaee SM, Sahebkar A. Ocular effects of sulfur mustard and therapeutic approaches. J Cell Biochem 2017;118:3549–60. [PubMed: 28106291]

[2]. Graham JS, Schoneboom BA. Historical perspective on effects and treatment of sulfur mustard injuries. Chem Biol Interact 2013;206:512–22. [PubMed: 23816402]

[3]. Graef I, Karnofsky DA, et al. The clinical and pathologic effects of the nitrogen and sulfur mustards in laboratory animals. Am J Pathol 1948;24:1–47. [PubMed: 18921345]

[4]. Watson AP, Griffin GD. Toxicity of vesicant agents scheduled for destruction by the chemical stockpile disposal program. Environ Health Perspect 1992;98: 259–80. [PubMed: 1486858]

[5]. Mansour Razavi S, Salamati P, Saghafinia M, Abdollahi M. A review on delayed toxic effects of sulfur mustard in Iranian veterans. Daru 2012;20:51. [PubMed: 23351810]

[6]. Panahi Y, Roshandel D, Sadoughi MM, Ghanei M, Sahebkar A. Sulfur mustard-induced ocular injuries: update on mechanisms and management. Curr Pharm Des 2017;23:1589–97. [PubMed: 27774903]

[7]. Rahmani H, Javadi I, Shirali S. Respiratory complications due to sulfur mustard exposure. Int J Curr Res Acad Rev 2016;4:143–9. [PubMed: 27668271]

[8]. Ganesan K, Raza SK, Vijayaraghavan R. Chemical warfare agents. J Pharm Bioallied Sci 2010;2:166–78. [PubMed: 21829312]

[9]. Dacre JC, Goldman M. Toxicology and pharmacology of the chemical warfare agent sulfur mustard. Pharmacol Rev 1996;48:289–326. [PubMed: 8804107]

[10]. Javadi MA, Yazdani S, Sajjadi H, Jadidi K, Karimian F, Einollahi B, et al. Chronic and delayed-onset mustard gas keratitis: report of 48 patients and review of literature. Ophthalmology 2005;112:617–25. [PubMed: 15808253]

[11]. Goswami DG, Tewari-Singh N, Agarwal R. Corneal toxicity induced by vesicating agents and effective treatment options. Ann N. Y Acad Sci 2016;1374: 193–201. [PubMed: 27327041]

[12]. Milhorn D, Hamilton T, Nelson M, McNutt P. Progression of ocular sulfur mustard injury: development of a model system. Ann N. Y Acad Sci 2010;1194:72–80. [PubMed: 20536452]

[13]. Amir A, Turetz J, Chapman S, Fishbeine E, Meshulam J, Sahar R, et al. Beneficial effects of topical anti-inflammatory drugs against sulfur mustard-induced ocular lesions in rabbits. J Appl Toxicol 2000;20(Suppl 1):S109–14. [PubMed: 11428620]

[14]. Javadi MA, Yazdani S, Kanavi MR, Mohammadpour M, Baradaran-Rafiee A, Jafarinasab MR, et al. Long-term outcomes of penetrating keratoplasty in chronic and delayed mustard gas keratitis. Cornea 2007;26:1074–8. [PubMed: 17893537]

[15]. Ruff AL, Jarecke AJ, Hilber DJ, Rothwell CC, Beach SL, Dillman 3rd JF. Development of a mouse model for sulfur mustard-induced ocular injury and long-term clinical analysis of injury progression. Cutan Ocul Toxicol 2013;32: 140–9. [PubMed: 23106216]

[16]. Ruff AL, Dillman 3rd JF. Sulfur mustard induced cytokine production and cell death: investigating the potential roles of the p38, p53, and NF-kappaB signaling pathways with RNA interference. J Biochem Mol Toxicol 2010;24: 155–64. [PubMed: 20143454]

[17]. Zheng R, Po I, Mishin V, Black AT, Heck DE, Laskin DL, et al. The generation of 4-hydroxynonenal, an electrophilic lipid peroxidation end product, in rabbit cornea organ cultures treated with UVB light and nitrogen mustard. Toxicol Appl Pharmacol 2013;272:345–55. [PubMed: 23845594]

[18]. Jain AK, Tewari-Singh N, Gu M, Inturi S, White CW, Agarwal R. Sulfur mustard analog, 2-chloroethyl ethyl sulfide-induced skin injury involves DNA damage and induction of inflammatory mediators, in part via oxidative stress, in SKH-1 hairless mouse skin. Toxicol Lett 2011;205:293–301. [PubMed: 21722719]

[19]. Sartori MF. New developments in the chemistry of war gases. Chem Rev 1951;48:225–57. [PubMed: 24540661]

[20]. Wang QQ Begum RA, Day VW, Bowman-James K. Sulfur, oxygen, and nitrogen mustards: stability and reactivity. Org Biomol Chem 2012;10:8786–93. [PubMed: 23070251]

[21]. Calvet JH, Feuermann M, Llorente B, Loison F, Harf A, Marano F. Comparative toxicity of sulfur mustard and nitrogen mustard on tracheal epithelial cells in primary culture. Toxicol vitro 1999;13:859–66.

[22]. Jesterj V, Ling J, Harbell J. Measuring depth of injury (DOI) in an isolated rabbit eye irritation test (IRE) using biomarkers of cell death and viability. Toxicol vitro 2010;24:597–604.

[23]. Folch J, Lees M, Sloane Stanley GH. A simple method for the isolation and purification of total lipides from animal tissues. J Biol Chem 1957;226: 497–509. [PubMed: 13428781]

[24]. Benton HP, Ivanisevic J, Mahieu NG, Kurczy ME, Johnson CH, Franco L, et al. Autonomous metabolomics for rapid metabolite identification in global profiling. Anal Chem 2015;87:884–91. [PubMed: 25496351]

[25]. McNutt P, Tuznik K, Nelson M, Adkins A, Lyman M, Glotfelty E, et al. Structural, morphological, and functional correlates of corneal endothelial toxicity following corneal exposure to sulfur mustard vapor. Invest Ophthalmol Vis Sci 2013;54:6735–44. [PubMed: 24045986]

[26]. Chaerkady R, Shao H, Scott SG, Pandey A, Jun AS, Chakravarti S. The keratoconus corneal proteome: loss of epithelial integrity and stromal degeneration. J Proteom. 2013;87:122–31.

[27]. Shetty R, Rao H, Khamar P, Sainani K, Vunnava K, Jayadev C, et al. Keratoconus screening indices and their diagnostic ability to distinguish normal from ectatic corneas. Am J Ophthalmol 2017;181:140–8. [PubMed: 28687218]

[28]. Qi H, Priyadarsini S, Nicholas SE, Sarker-Nag A, Allegood J, Chalfant CE, et al. Analysis of sphingolipids in human corneal fibroblasts from normal and keratoconus patients. J Lipid Res 2017;58:636–48. [PubMed: 28188148]

[29]. Netto MV, Mohan RR, Ambrosio R Jr, Hutcheon AE, Zieske JD, Wilson SE. Wound healing in the cornea: a review of refractive surgery complications and new prospects for therapy. Cornea 2005;24:509–22. [PubMed: 15968154]

[30]. Kronschlager M, Talebizadeh N, Yu Z, Meyer LM, Lofgren S. Apoptosis in rat cornea after in vivo exposure to ultraviolet radiation at 300 nm. Cornea 2015;34:945–9. [PubMed: 26075458]

[31]. Lu L, Wang L, Shell B. UV-induced signaling pathways associated with corneal epithelial cell apoptosis. Invest Ophthalmol Vis Sci 2003;44:5102–9. [PubMed: 14638704]

[32]. Torricelli AA, Santhanam A, Wu J, Singh V, Wilson SE. The corneal fibrosis response to epithelial-stromal injury. Exp Eye Res 2016;142:110–8. [PubMed: 26675407]

[33]. Wilson SE, Mohan RR, Netto M, Perez V, Possin D, Huang J, et al. RANK, RANKL, OPG, and M-CSF expression in stromal cells during corneal wound healing. Invest Ophthalmol Vis Sci 2004;45:2201–11. [PubMed: 15223796]

[34]. Kim TI, Pak JH, Tchah H, Lee SA, Kook MS. Ceramide-induced apoptosis in rabbit corneal fibroblasts. Cornea 2005;24:72–9. [PubMed: 15604870]

[35]. Rizvi F, Heimann T, Herrnreiter A, O'Brien WJ. Mitochondrial dysfunction links ceramide activated HRK expression and cell death. PLoS One 2011;6:e18137.

[36]. Bazan H, Ottino P. The role of platelet-activating factor in the corneal response to injury. Prog Retin Eye Res 2002;21:449–64. [PubMed: 12207945]

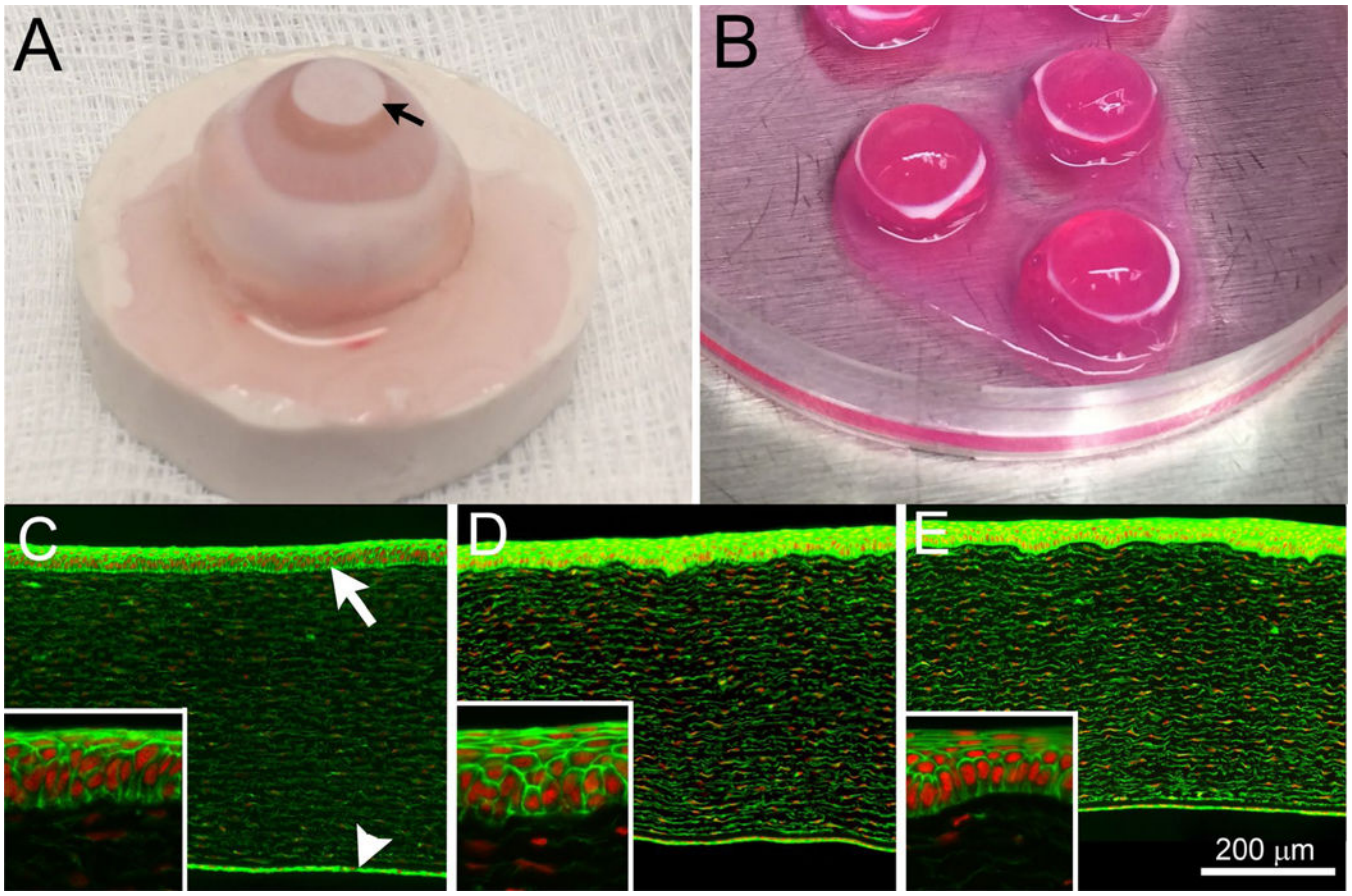

Figure 1. Isolated rabbit eye model.

(**A**) Isolated rabbit eyes were exposed to NM by applying a sterile 5 mm diameter filter disk (arrow) impregnated with 10 μl of sterile water (control) or NM solution to the cornea for 5, 10 or 15 min. At the end of the exposure period, the cornea (and 2–3mm of surrounded sclera) was surgically isolated, placed on top of agar posts and organ cultured at 37 °C (**B**) for 3, 24 or 48 h. Rabbit corneas exposed to sterile water for 5, 10 or 15 min, showed no differences in epithelial thickness, stromal thickness and stromal cell viability after 3 (**C**), 24 (**D**) or 48 h (**E**) of organ culture. Insets show higher magnification of the corneal epithelium. Live cells and nuclei were identified by phalloidin (green) and DAPI (red) stains, respectively. The corneal epithelium (white arrow) and posterior corneal endothelium (white arrowhead) are shown.

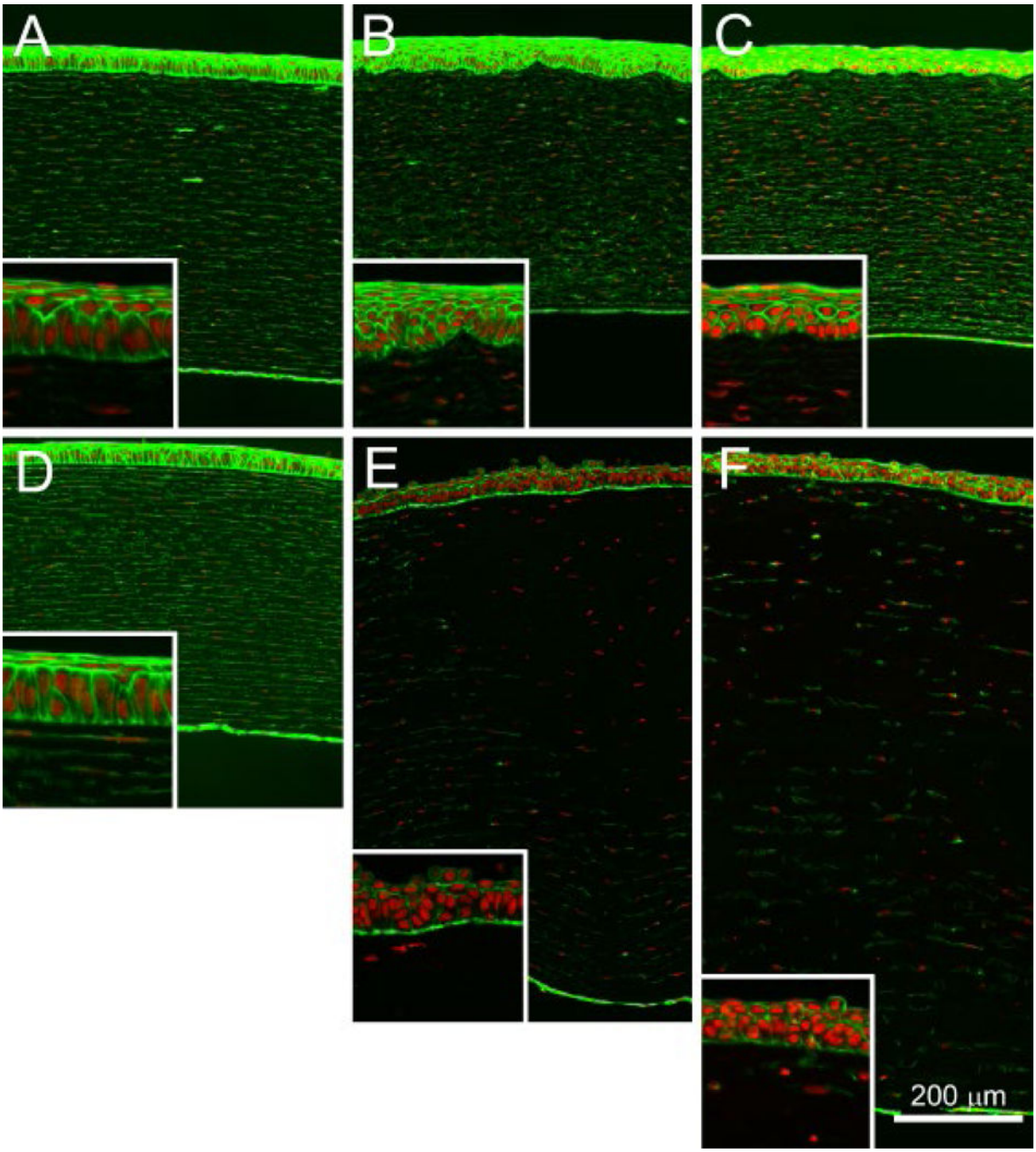

Figure 2. Histological changes induced by nitrogen mustard exposure.

Rabbit corneas were exposed for 5 min to 1 mg/ml (**A–C**) or 10 mg/ml (**D–F**) NM and subjected to organ culture for an additional 3 h (**A** and **D**), 24 h (**B** and **E**) or 48 h (**C** and **F**). Intact cells and nuclei were identified by phalloidin (green) and DAPI (red) stains, respectively.

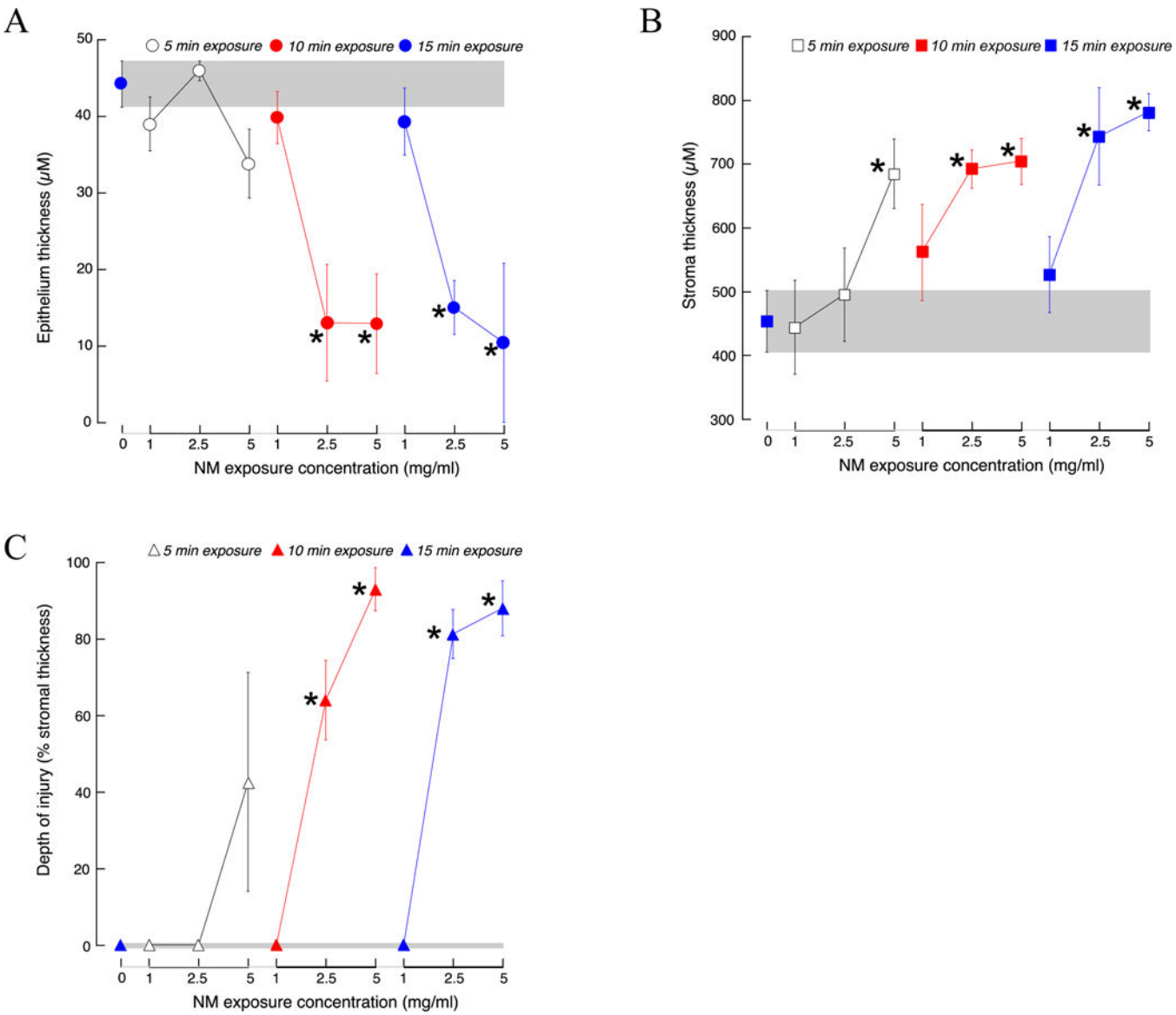

Figure 3: Effects of nitrogen mustard exposure concentration and duration on extent of corneal injury.

Isolated rabbit corneas were exposed to sterile water (control) for 15 min or various concentrations (1, 2.5, 5 mg/ml) of nitrogen mustard (NM) for 5 (open symbol), 10 (red symbol) or 15 (blue symbol) min. The thickness of the corneal epithelium (**A**) and stroma (**B**), and the stromal depth of injury (expressed as a percentage of the stromal thickness, **C**) were measured 24 h after the end of the exposure period. Data are presented as mean ± SD from 3 to 4 rabbits.

*P < 0.05, one-way ANOVA, compared to control (0 mg/ml NM).

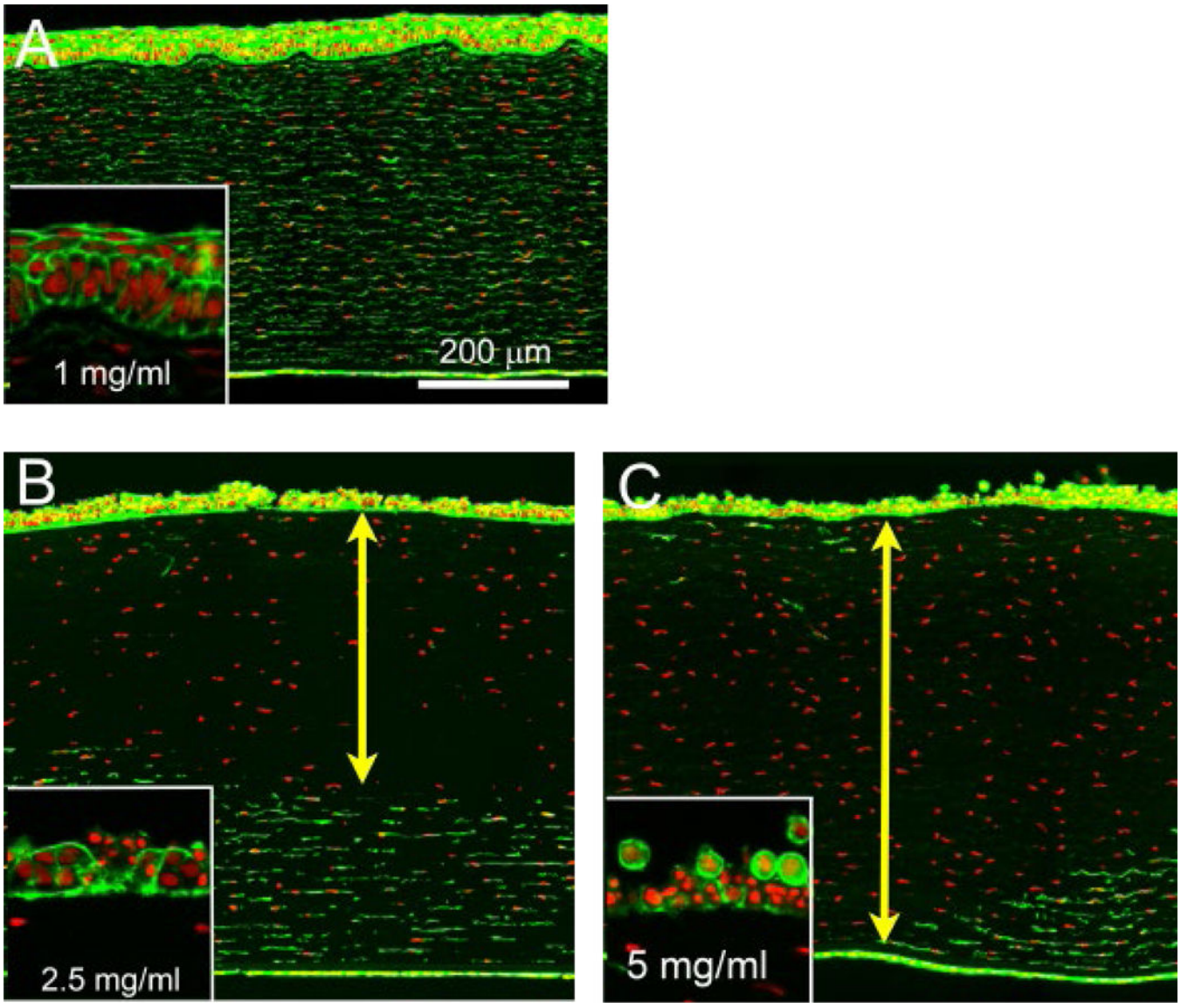

Figure 4. Effect of NM concentration on depth of injury.

Rabbit corneas exposed for 10 min to 1 (**A**), 2.5 (**B**) or 5 (**C**) mg/ml NM and subjected to organ culture for an additional 24 h showed a range of corneal damage. Live cells and nuclei were identified by phalloidin (green) and DAPI (red) stains, respectively. The line with double arrowheads shows the region of dead stromal cells.

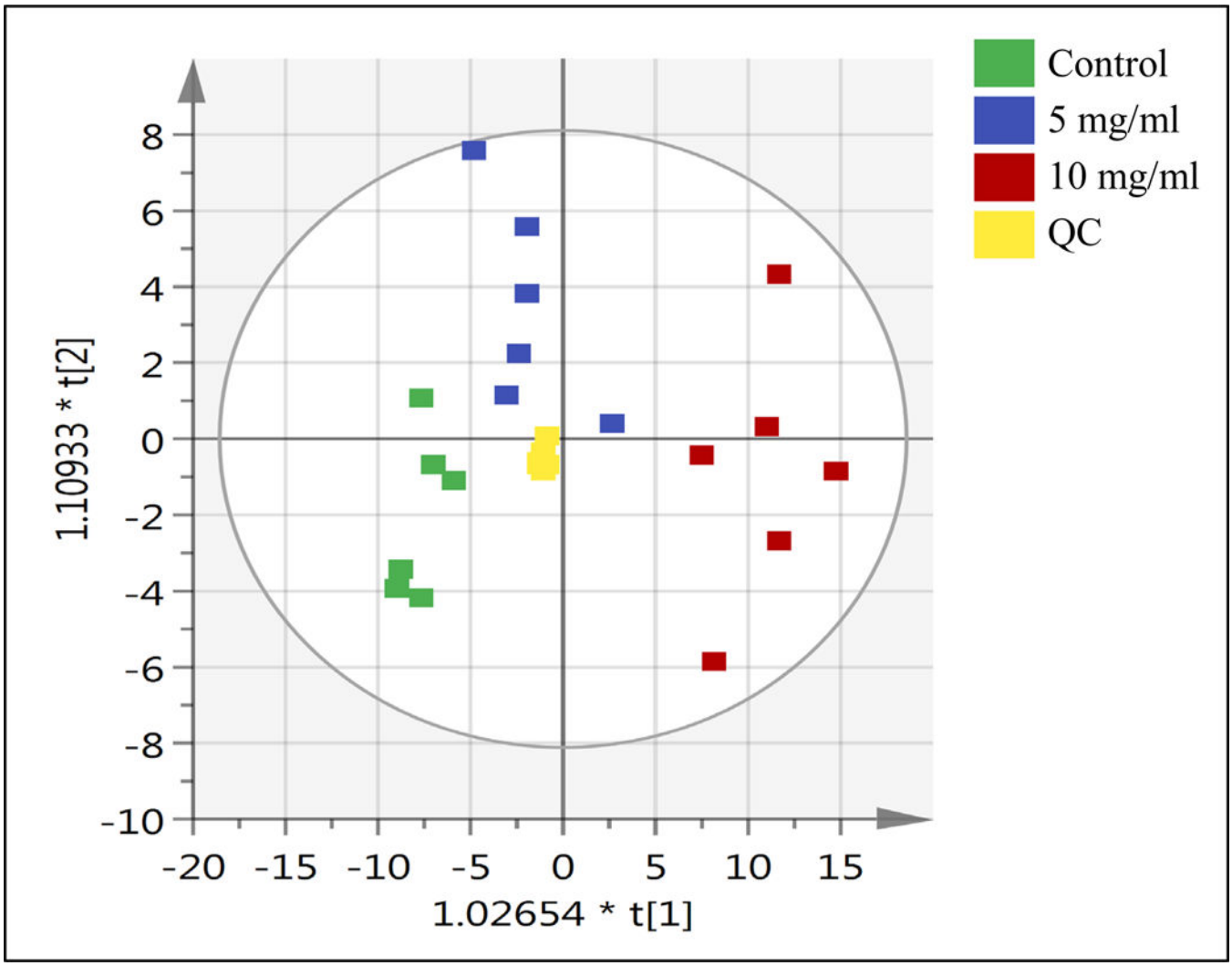

Figure 5: Orthogonal partial least square discriminant analysis (OPLS-DA) of corneal metabolites induced by nitrogen mustard exposure.

Isolated rabbit corneas were exposed to sterile water or various concentrations of nitrogen mustard (NM) for 15 min. The OPLS-DA plot shows separation between the following groups: sterile water (Control), 5 mg/ml NM ( ) 10 mg/ml NM ( ) and pooled sample (QC,).

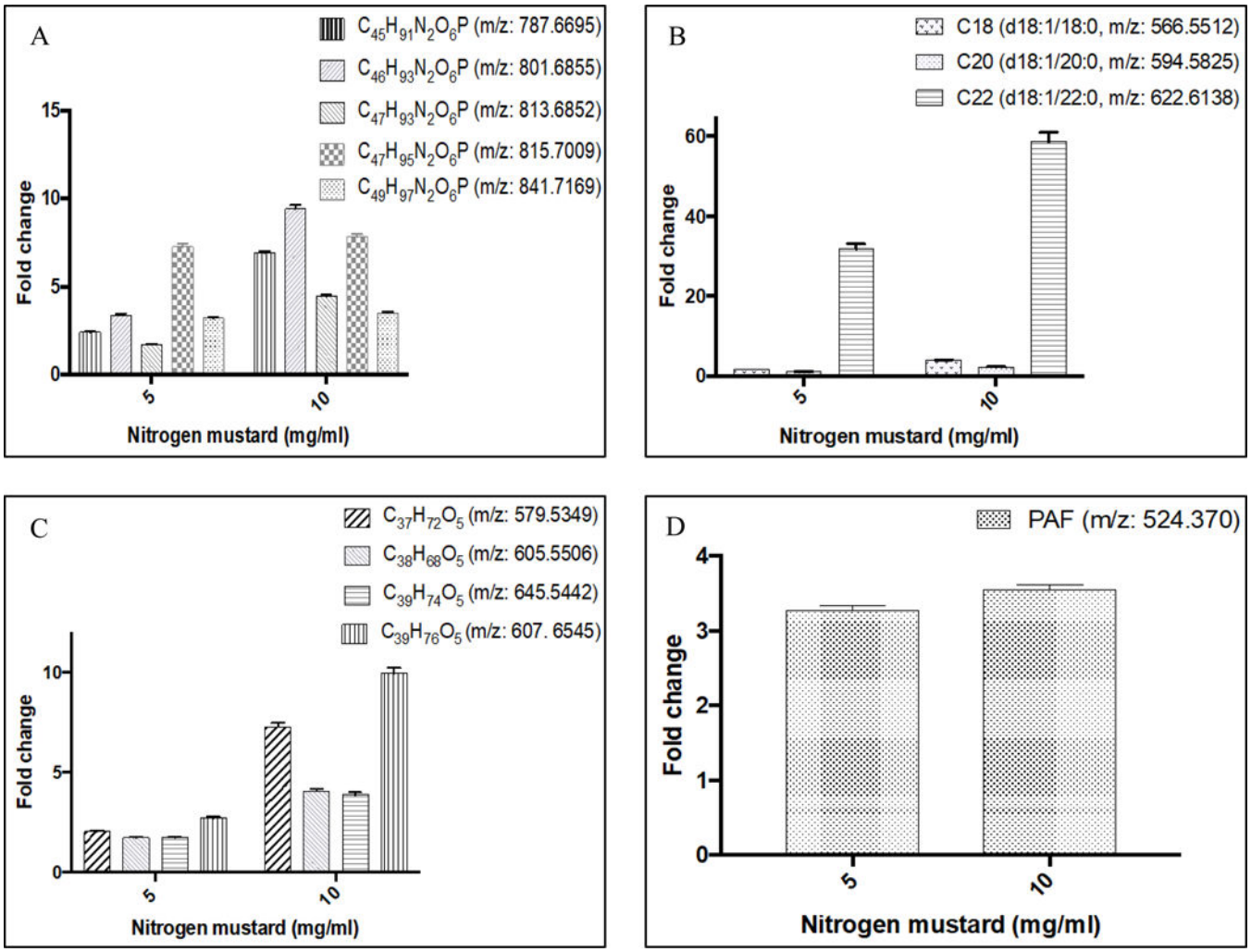

Figure 6: Changes in lipid metabolites induced by nitrogen mustard exposure.

Isolated rabbit corneas were exposed to sterile water (control) or various concentrations (5 or 10 mg/ml) of nitrogen mustard (NM) for 15 min. Lipid extracts of corneal tissue were subjected to untargeted lipidomics and metabolites were putatively identified using the LipidBlast database. Results are shown for identified sphingomyelins (**A**), ceramides (**B**), diacylglycerols (**C**) and platelet activator factor (PAF, **D**). Levels of metabolites are expressed as fold change of control. Data represent mean and associated %CV from 6 corneas. All metabolites present in NM-treated corneas were significantly different ($P < 0.05$, one-way ANOVA) from control.

Table 1.

Sphingomyelin metabolites putatively identified in nitrogen mustard-exposed corneal tissue extracts.

Isolated rabbit corneas were exposed to sterile water (control) or various concentrations (5 or 10 mg/ml) of nitrogen mustard (NM) for 15 min. Lipid extracts of corneal tissue were subjected to untargeted metabolomics and metabolites were tentatively identified using the LipidBlast database. Metabolites were tentatively identified using the LipidBlast database. Retention time (min), positively-charged mass (M + H), tentative compound ID, and formula are shown.

Retention time (min)	Positively-charged mass (M + H)	Compound ID	Formula	Fold-change in levels (relative to control)	
				5 mg/ml NM	10 mg/ml NM
13.52	813.6852	d16:1/26:1	$C_{47}H_{93}N_2O_6P$	2.1	4.2
		d18:1/24:1			
13.57	787.6695	d14:0/26:1	$C_{45}H_{91}N_2O_6P$	3.1	7.0
		d16:1/24:0			
		d18:1/22:0			
		d16:0/24:1			
		d14:1/26:0			
13.85	801.6855	d17:0/24:1	$C_{46}H_{93}N_2O_6P$	4.4	9.3
		d17:1/24:0			
		d19:1/22:0			
		d15:0/26:1			
		d15:1/26:0			
14.05	841.7690	d18:1/26:1	$C_{49}H_{97}N_2O_6P$	2.2	3.2
14.10	815.7009	d18:1/24:0	$C_{47}H_{95}N_2O_6P$	2.8	7.7
		d16:1/26:0			
		d18:0/24:1			
		d16:0/26:1			